Medicago truncatula Ferroportin2 mediates iron import into nodule symbiosomes

Viviana Escudero, Isidro Abreu, Manuel Tejada-Jiménez, Elena Rosa-Núñez, Julia Quintana, Rosa Isabel Prieto, Camille Larue, Jiangqi Wen, Julie Villanova, Kirankumar S. Mysore, et al.

1   *Medicago truncatula* **Ferroportin2 mediates iron import into nodule symbiosomes**

2   Viviana Escudero[a], Isidro Abreu[a], Manuel Tejada-Jiménez[a], Elena Rosa-Núñez[a], Julia

3   Quintana[b], Rosa Isabel Prieto[a], Camille Larue[c] Jianqi Wen[d], Julie Villanova[e], Kirankumar

4   S. Mysore[d], José M. Argüello[b], Hiram Castillo-Michel[f] Juan Imperial[g], Manuel González-

5   Guerrero[a,h,1]

6   [a] Centro de Biotecnología y Genómica de Plantas (UPM-INIA), Universidad Politécnica de

7   Madrid, 28223 Pozuelo de Alarcón (Madrid), Spain.

8   [b] Worcester Polytechnic Institute, Worcester MA01609, USA.

9   [c] EcoLab, Université de Toulouse, CNRS, Toulouse, France

10   [d] Noble Research Institute, Ardmore, OK73401, USA.

11   [e] ID16 Beamline. European Synchrotron Radiation Facility, Grenoble 38043, France.

12   [f] ID21 Beamline. European Synchrotron Radiation Facility, Grenoble 38043, France.

13   [g] Instituto de Ciencias Agrarias, Consejo Superior de Investigaciones Científicas, 28006

14   Madrid, Spain.

15   [h] Escuela Técnica Superior de Ingeniería Agronómica, Alimentaria y de Biosistemas,

16   Universidad Politécnica de Madrid, 28040 Madrid, Spain.

17

18   [1] Address correspondence to manuel.gonzalez@upm.es

19

20   Short Title: MtFPN2 delivers iron to symbiosomes

21

22   The author responsible for distribution of materials integral to the findings presented in this

23   article in accordance with the policy described in the Instruction for Authors

24   (www.plantcell.org) is: Manuel González-Guerrero (manuel.gonzalez@upm.es).

25

26

1

ABSTRACT

Iron is an essential cofactor for symbiotic nitrogen fixation. It is required by many of the enzymes facilitating the conversion of N_2 into NH_4^+ by endosymbiotic bacteria living within root nodule cells, including signal transduction proteins, O_2 homeostasis systems, and nitrogenase itself. Consequently, host plants have developed a transport network to deliver essential iron to nitrogen-fixing nodule cells. Model legume *Medicago truncatula Ferroportin2* (*MtFPN2*) is a nodule-specific gene that encodes an iron-efflux protein. MtFPN2 is located in intracellular membranes in the nodule vasculature, and in the symbiosome membranes that contain the nitrogen-fixing bacteria in the differentiation and early-fixation zones of the nodules. Loss-of-function of *MtFPN2* leads to altered iron distribution and speciation in nodules, which causes a reduction in nitrogenase activity and in biomass production. Using promoters with different tissular activity to drive *MtFPN2* expression in *MtFPN2* mutants, we determined that MtFPN2-facilitated iron delivery across symbiosomes is essential for symbiotic nitrogen fixation, while its presence in the vasculature does not seem to play a major role in in the conditions tested.

54 **INTRODUCTION**

55   Iron is an essential cofactor for enzymes participating in almost every plant
56 physiological process, including photosynthesis, respiration, and stress tolerance
57 (Marschner, 2011). Consequently, when lacking, a plethora of iron-dependent processes is
58 affected. Damaging as low iron levels are, so are slightly higher ones. In that situation, iron
59 becomes toxic, catalysing the production of free radicals in Fenton-style reactions and
60 competing with other essential metal nutrients for the active site of proteins (Goldstein et
61 al., 1993; Lin et al., 2011). To maintain iron homeostasis within these narrow physiological
62 levels, plants have developed a complex system to optimize iron uptake and delivery from
63 soil, while preventing toxicity. This system involves metal transporters that recover this
64 nutrient from soil and deliver it to shoots and seeds (Korshunova et al., 1999; Curie et al.,
65 2001; Vert et al., 2002; Morrissey et al., 2009; Zhai et al., 2014), small soluble molecules
66 that coordinate iron and keep it soluble in plant fluids (von Wiren et al., 1999; Rogers and
67 Guerinot, 2002; Roschzttardtz et al., 2011; Flis et al., 2016), and a complex regulatory
68 network (Colangelo and Guerinot, 2004; Long et al., 2010; Sivitz et al., 2012; Kumar et al.,
69 2017; Grillet et al., 2018). While in most vegetative growing plants, the main iron sinks are
70 the leaves, legumes may have additional ones in differentiated root organs known as
71 nodules (Brear et al., 2013; González-Guerrero et al., 2014). Representing just 5% of the
72 total biomass of the plant, nodules contain a large part of the plant iron content (González-
73 Guerrero et al., 2014; Tejada-Jiménez et al., 2015). Therefore, it is to be expected that
74 legumes have adapted their pre-existing iron homeostasis systems to accommodate nodule
75 development and function.

76   Nodules are the result of the interaction between legumes and rhizobia, a diverse
77 group of soil bacteria capable of converting, fixing, N_2 into NH_4^+ when in symbiosis
78 (Downie, 2014). Following a complex signal exchange between the symbionts (Vernié et
79 al., 2015), nodule primordia emerge from the roots by proliferation of pericycle and inner
80 cortex cells (Xiao et al., 2014). While the nodule develops, rhizobia in the root surface are
81 surrounded by a root hair that invaginates and directs, via an infection thread, the bacteria
82 from the root exterior to the inner nodule regions (Gage, 2002), where they are released in
83 an endocytic-like process (Limpens et al., 2009; Huisman et al., 2012). Within these
84 pseudo-organelles (symbiosomes), rhizobia differentiate into bacteroids (Sutton et al.,

3

85   1981; Kereszt et al., 2011), and start fixing nitrogen, transferring fixed NH_3 to the host

86   plant in exchange for photosynthates and mineral nutrients (Udvardi and Poole, 2013).

87   Nodules can be classified according to their development in determinate and indeterminate

88   (Sprent, 2007). The former, as illustrated by soybean nodules, has a limited growth, while

89   the later (developed by pea or *Medicago*), maintains the apical meristem and has a longer

90   growth period. Due to this indeterminate nodule growth, four nodule zones are established,

91   tracing along its length the developmental stages of nodule maturation. These zones are: the

92   meristem (zone I), the zone where the nodule cells are infected by rhizobia and they

93   differentiate into bacteroids (zone II), the N_2 fixation zone (zone III), and in nodules of a

94   certain age, the senescent zone (zone IV) (Vasse et al., 1990). In addition, some authors

95   also differentiate an interzone between zones II and III in which O_2 levels drop and

96   nitrogenase is starting to be synthesized (Roux et al., 2014).

97   Nodule development is highly sensitive to iron levels, as suggested by its abundance

98   in these organs. Iron deficiency limits nodule number and maturation, as well as reduces

99   nitrogen fixation rates (O'Hara et al., 1988; Tang et al., 1990; Tang et al., 1992). This is the

100   consequence of many of the key enzymes involved in nodulation and nitrogen fixation

101   being ferroproteins synthesized at high levels (Brear et al., 2013; González-Guerrero et al.,

102   2014). For instance, heme-containing NADPH-oxidases are important for nodule initiation

103   and development (Montiel et al., 2012; Montiel et al., 2016). Nitrogenase, the critical

104   enzyme for nitrogen fixation, is a protein complex with 34 iron atoms in the form of iron-

105   sulfur (Fe-S) clusters and the unique iron-molybdenum cofactor (FeMoco) (Rubio and

106   Ludden, 2005). This enzyme is irreversibly inhibited by O_2, while bacteroids must carry out

107   an aerobic metabolism (Preisig et al., 1996b). To make both processes compatible, legumes

108   express leghemoglobin (20% of the total nodule protein) which binds O_2 with great affinity

109   (Appleby, 1984). This oxygen can be recovered and used by high-affinity rhizobial

110   cytochrome *c* oxidases (iron-copper proteins) (Preisig et al., 1996a; Preisig et al., 1996b). In

111   addition, a number of other iron-proteins are required for free radical control, cofactor

112   assembly, and general metabolic processes (Dalton et al., 1998; Rubio et al., 2004; Rubio

113   and Ludden, 2005; González-Guerrero et al., 2014).

114   To ensure the reinforced iron supply that symbiotic nitrogen fixation requires,

115   nodulation elicits the iron-deficiency response characteristic of dicots (Terry et al., 1991):

116   lowering the pH of the rhizosphere to increase Fe^{3+} solubility, activating ferroreductase

117   activities to reduce Fe^{3+} to Fe^{2+}, and inducing the expression of Fe^{2+} importers of the ZIP

118   (Zrt1-, Irt1-like Proteins) and Nramp (Natural Resistance Associated Macrophage Protein)

119   transporter families (Andaluz et al., 2009; Kobayashi and Nishizawa, 2012). Once iron is in

120   the plant, it symplastically or apoplastically reaches the endodermis from where it will be

121   delivered by the vasculature to shoots and nodules. At the nodules, iron is released in the

122   apoplast of the infection zone of the nodule (Rodríguez-Haas et al., 2013), where it is kept

123   soluble as iron-citrate (Kryvoruchko et al., 2018), the most abundant complex in root to

124   shoot iron transport and when transferring it across symplastically disconnected tissues

125   (Durrett et al., 2007; Roschzttardtz et al., 2011). Iron uptake into the infected cells of

126   *Medicago truncatula* is mediated primarily by MtNramp1, a transporter expressed in late

127   zone II and interzone and located in the plasma membrane (Tejada-Jiménez et al., 2015).

128   Transport into the symbiosomes is likely also facilitated by citrate, as indicated by the

129   requirement of citrate efflux protein MtMATE67 (Kryvoruchko et al., 2018). However, this

130   protein does not transport iron-citrate complexes, and therefore, another system must exist

131   for iron translocation. Different candidates have been proposed to be responsible for iron

132   delivery into the symbiosomes. The first was *Glycine max* Nramp protein GmDMT1

133   (Kaiser et al., 2003). However, although this protein was located in symbiosomes, its

134   direction of transport would be into the cytosol, as with all characterized Nramp proteins

135   (Nevo and Nelson, 2006). VIT1-CCC1-like protein SEN1 is another candidate to carry out

136   this role (Hakoyama et al., 2012), but although the direction in which iron is transported by

137   these proteins would be compatible (Li et al., 2001), there is no definitive evidence of a

138   symbiosome localization. Alternatively, a member of the ferroportin family (also known as

139   IREG proteins) could also be involved.

140   Ferroportins are membrane proteins that extrude iron from the cytosol, either

141   outside the cell or into organelle (Morrissey et al., 2009; Drakesmith et al., 2015). In plants,

142   ferroportins have been associated to iron delivery into the xylem (Morrissey et al., 2009).

143   Interestingly, this is a process that would be coupled to MATE-mediated citrate efflux

144   (FRD3 in *A. thaliana*) (Durrett et al., 2007), as iron is kept soluble in the xylem as an iron-

145   citrate complex (López-Millán et al., 2000; Durrett et al., 2007). Considering the functional

146   association of ferroportins and citrate efflux proteins in the xylem, we hypothesized that a

5

147   similar relationship would be established between nodule-specific citrate efflux protein

148   MtMATE67 and a ferroportin to deliver iron to nodule apoplast and to symbiosomes. As a

149   result, we have identified and characterized MtFPN2 (*Medtr4g013240*), one of the three

150   ferroportin-like genes encoded in the *M. truncatula* genome, and the only one with a

151   nodule-specific expression. MtFPN2 is located in the intracellular compartments in the

152   endodermis, and associated to symbiosomes in the infected cells. Mutation of *MtFPN2*

153   results in a severe reduction of nitrogenase activity, and in mis-localization of iron in the

154   nodules. These results support a role of MtFPN2 in iron delivery for symbiotic nitrogen

155   fixation.

156

RESULTS

MtFPN2 is expressed in the nodule vasculature and interzone

159   Three ferroportin-like sequences could be found in the genome of *M. truncatula*:

160   *Medtr1g084140* (*MtFPN1*), *Medtr4g013240* (*MtFPN2*), and *Medtr4g013245* (*MtFPN3*).

161   Among them, *MtFPN2* was the only ferroportin to have a nodule-specific transcription in

162   the conditions tested (Figure 1A; Supplemental Figure 1). To determine the area of the

163   nodule where *MtFPN2* was expressed, the 2,144 bp DNA region immediately upstream of

164   *MtFPN2* start codon was used to drive the expression of the reporter *β-glucuronidase* (*gus*)

165   gene. After 28 days-post-inoculation (dpi), GUS activity was detected in a specific nodule

166   band close to the apical region, and in longitudinal bands along its major axis (Figure 1B).

167   Longitudinal sections of nodules showed that the apical GUS-activity region corresponded

168   to the late infection zone, interzone and early fixation zone (Figure 1C). Nodule cross

169   sections showed GUS activity in the nodule vasculature (Figure 1D). In these cross

170   sections, the lack of expression of *MtFPN2* in the matured fixation zone was also

171   confirmed.

MtFPN2-HA is located in vascular intracellular compartments and in the symbiosomes

174   Ferroportins have been associated to iron efflux from the cytosol (Kaplan, 2002).

175   Their specific functional role is largely derived from the specific subcellular localization of

6

176 each protein. Should it be associated to the plasma membrane, its likely role would be iron
177 export for long-distance trafficking, such as FPN1 in enterocytes, or FPN1 in endodermal
178 cells (McKie et al., 2000; Morrissey et al., 2009). Alternatively, an intracellular localization
179 associated to organelle would mean a role in iron storage or metalation of specific
180 ferroproteins (Morrissey et al., 2009; Drakesmith et al., 2015). To determine the subcellular
181 distribution of MtFPN2 and gain insights into its function, three hemagglutinin (HA)
182 epitopes where fused to its C-terminus. The expression of this cassette was driven by the
183 same region previously used for the *MtFPN2*$_{prom}$::*gus* fusions. Protein localization was
184 initially determined by confocal microscopy in which the epitopes were detected by an anti-
185 HA monoclonal primary antibody and an Alexa594-conjugated (red) secondary antibody.
186 To facilitate visualization, the transformed plants were inoculated with a GFP-expressing
187 *Sinorhizobium meliloti* strain (green) and the sections stained with DAPI (blue) to visualize
188 DNA. Figure 2A shows that MtFPN2-HA localization corresponded to the expression
189 profile detected with the *MtFPN2*$_{prom}$::*gus* fusions. A detailed view of the vascular region
190 revealed that MtFPN2-HA was located in the endodermis, pericycle and in the vascular
191 parenchyma, occupying large areas of the cytosol (Figure 2B). Visualization of infected
192 cells in the differentiation zone also showed an intracellular localization of MtFPN2-HA,
193 closely related to the symbiosomes (Figure 2C). To confirm this putative symbiosome
194 localization, *M. truncatula* plants were transformed with a C-terminal GFP-fusion of
195 *MtFPN2* driven by its own promoter and inoculated with a mCherry expressing *S. meliloti*.
196 Symbiosomes isolated from these nodules showed co-localization of rhizobia and MtFPN2-
197 GFP (Supplemental Figure 2). To further verify the symbiosome localization of MtFPN2-
198 HA, a gold-conjugated secondary antibody was used to determine the distribution of HA-
199 tagged proteins using transmission electron microscopy. As indicated by the confocal
200 microscopy assays, gold particles were associated to symbiosome membranes (Figure 2D).
201 The same approach showed gold particles concentrated in large intracellular membrane
202 systems, very likely the endoplasmic reticulum in endodermal and vascular parenchyma
203 cells (Figure 2D). To confirm that none of these observations were artifactual, controls for
204 autofluorescence of the tagged proteins and specificity of the antibodies were carried out
205 (Supplemental Figure 3).

206 **MtFPN2 is an iron efflux protein**

7

207   To confirm that MtFPN2 was capable of transporting iron, we tested its ability to

208   restore the wild-type growth of a yeast mutant lacking the CCC1 protein. This transporter

209   introduces excess cytosolic iron into the vacuole to prevent toxicity (Li et al., 2001). Loss

210   of CCC1 function resulted in lower iron tolerance when the media was supplemented with

211   2.5 mM $FeSO_4$. However, when this strain was transformed with a plasmid expressing the

212   coding sequence of *MtFPN2*, the sensitivity of the mutant strain to high iron was

213   diminished (Figure 3), suggesting that MtFPN2 was able to participate in its detoxification.

214   Addition of the HA-tag used for the immunolocalization studies did not affect MtFPN2

215   activity in yeast (Supplemental Figure 4).

216   **MtFPN2 is required for nitrogenase activity in nodules**

217   Should MtFPN2 be responsible for iron delivery to the nodules, its mutation should

218   lead to a reduction of nitrogenase activity, as a consequence of an iron-limited cofactor

219   synthesis. To explore this possibility, the *Tnt1* insertion mutant NF11374 (*fpn2-1*) was

220   obtained from the Noble Research Institute (Tadege et al., 2008). This line has an insertion

221   in the fourth exon of *MtFPN2* (Figure 4A), resulting in no transcript being detected by RT-

222   PCR. *MtFPN2* loss-of-function had no significant effect on plant growth or chlorophyll

223   content when the plants had not been inoculated and nitrogen was provided as ammonium

224   nitrate in the nutrient solution (Supplemental Figure 5). However, when the plants were

225   inoculated and nitrogen had to be obtained from the endosymbiotic rhizobia, removing

226   *MtFPN2* function led to severe growth reduction (Figure 4B). Nodule development was

227   also altered, with a large portion (64%) of the nodules having white colour (Figure 4C, 4D),

228   indicative of non-functionality. Closer observation of these nodules using either toluidine

229   blue-stained sections or tomographic reconstructions from X-ray analyses, showed that the

230   white *fpn2-1* nodules did not develop the fixation zones further than a few cell layers

231   (Supplemental Figure 6), and that even the fewer nodules with a pink-colour had a reduced

232   Zone III. In addition, the symbiosomes appeared disorganized in the cytosol of *fpn2-1*

233   nodule cells, with a number of vacuoles, in contrast to the ordered, radial and peripheral

234   distribution in the wild type plants. As expected by the plant and nodule phenotypes,

235   biomass production was significantly lower in *fpn2-1* plants than in wild-type plants

236   (Figure 4E). Nitrogen fixation capabilities (nitrogenase activity) of the mutant nodules were

237   approximately 80% lower than those from wild-type plants (Figure 4F). These phenotypes

238   were the likely result of iron not reaching the nodules in high-enough levels, as indicated by

239   the lower iron content of *fpn2-1* nodules (Figure 4G). Introducing into *fpn2-1* the coding

240   sequence of *MtFPN2* regulated by the 2,144 bp region upstream its start codon restored the

241   wild-type phenotype. However, fortifying the nutrient solution with additional iron did not

242   have the same effect (Supplemental Figure 7).

243   Consistent with the phenotype arising from altered iron delivery to the nodules,

244   synchrotron-based micro-X-ray fluorescence studies of wild-type and *fpn2-1* nodules

245   showed altered distribution of this element (Figure 5A). *MtFPN2* mutation led to less iron

246   being allocated to the early fixation zones of the nodules, in those cases where the region

247   was marginally developed (pink *fpn2-1* nodules). In the case of fully white nodules, no iron

248   distribution indicative of ordered symbiosomes (iron-rich ring-like structures) was

249   observed, consistent with no functional zone III being fully developed. This alteration in

250   iron distribution had an impact on iron speciation as determined by micro-X-ray Absorption

251   Near-Edge Spectroscopy (μXANES) on nodule sections. Different iron spectra were

252   obtained from wild-type and mutant nodules (Figure 5B). Principal component analyses of

253   the obtained spectra in the infection/differentiation zone, fixation zone and vascular region

254   showed great iron speciation variation between wild-type and white *fpn2-1* nodules (Figure

255   5B). Interestingly, iron speciation in pink *fpn2-1* nodules showed an intermediate state

256   midway from wild-type and white *fpn2-1* nodules. Although the complex iron speciation in

257   nodules and the lack of a suitable number of spectra from many of these forms precludes a

258   detailed description of the precise chemical species present in these organs, it was

259   interesting to notice that the proportion of iron coordinated by sulfur (Fe-S clusters,

260   including the iron-molybdenum cofactor of nitrogenase) was different in wild type, pink

261   *fpn2-1*, and white *fpn2-1* nodules (Supplemental Table 1).

262   Considering the dual localization of MtFPN2 in the vasculature and in the

263   symbiosomes, the reported phenotypes could be due to either iron not being released from

264   the vessels and/or from it not getting across the symbiosome membrane. In an attempt to

265   separate both causes, *MtFPN2* coding sequence was cloned under the *MtMOT1.3* promoter,

266   a nodule-specific gene that we had previously located in the interzone and early fixation

267   zone (Tejada-Jiménez et al., 2017). Mutants *fpn2-1* were transformed with this construct to

268   test whether expressing *MtFPN2* only in the nodule cortex was sufficient to restore the

269   phenotype. As shown in Figure 6, *MOT1.3$_{prom}$* driven expression of *MtFPN2* resulted in a

270   partial improvement of plant growth (Figure 6A), with the development of functional pink

271   nodules in significantly higher numbers than *fpn2-1* (Figures 6B and C). Overall, these

272   plants showed improved biomass production compared to *fpn2-1* (Figure 6D), albeit not

273   enough to reach wild-type levels. The improved iron delivery to *fpn2-1* led to significantly

274   higher nitrogen fixation rates per nodule (Figure 6E). In contrast, when *MtFPN2* expression

275   was driven by the promoter of vascular gene *MtNOOT1* (Magne et al., 2018), no significant

276   differences were observed in terms of biomass production, nodule development, or

277   nitrogenase activity with those that do not express it at all (Supplemental Figure 8).

278

DISCUSSION

280   Symbiotic nitrogen fixation carried out by the legume-rhizobia systems is one of the

281   main sources of assimilable nitrogen in natural ecosystems and in agrosystems (Vance,

282   2001; Herridge et al., 2008). A key element in crop rotation strategies to increase nitrogen

283   content in soils, symbiotic nitrogen fixation can minimize the use of polluting and

284   expensive nitrogen fertilizers. Unveiling the molecular bases of this process is critical to

285   improve nitrogen fixation rates and to introduce these capabilities to non-legume crops

286   (Oldroyd and Dixon, 2014; Mus et al., 2016). However, for symbiotic nitrogen fixation to

287   be efficiently used in sustainable agriculture or to extend it to other systems, close attention

288   has to be paid to the mechanisms of delivery of essential, limiting nutrients, such as iron.

289   Nitrogen fixation, oxygen homeostasis, reactive oxygen species production and

290   control, and several other nodule physiological processes rely on iron (Brear et al., 2013;

291   González-Guerrero et al., 2014; González-Guerrero et al., 2016), a limiting nutrient in large

292   areas of the world (Hirschi, 2009; White and Broadley, 2009). Therefore, nodules must

293   ensure a steady supply of this element. While free-living diazotrophs can obtain iron

294   directly from soil, endosymbiotic ones must obtain it from the host (Rodríguez-Haas et al.,

295   2013; Udvardi and Poole, 2013). This process was likely adapted from the pre-existing

296   long-distance iron transport systems. Consequently, we might expect similar mechanisms

297   to those dedicated for iron delivery to the shoots, with the added handicap of the nodules

298   becoming a second sink of an already scarce nutrient. Further supporting this hypothesis is

10

299 the existence of a nodule-specific iron-regulated citrate efflux protein that showcases the

300 importance of iron-citrate complexes in apoplastic iron solubility and in iron supply to

301 symbiosomes (Kryvoruchko et al., 2018). Since ferroportins were associated to citrate-

302 mediated long-distance iron supply (Morrissey et al., 2009), we speculated on a putative

303 role for these proteins in symbiotic nitrogen fixation.

304 Model legume *M. truncatula* encodes three ferroportin-like proteins. One of them,

305 MtFPN1, closely resembles the Mar1 protein located in the chloroplasts of Arabidopsis,

306 that plays an undefined role in iron homeostasis in plants, as well as serving as entry-point

307 for antibiotics (Conte et al., 2009). Similarly to *Mar1*, *MtFPN1* was expressed in the whole

308 plant. The other two are orthologues to *A. thaliana* FPN1 and FPN2. While *MtFPN3* was

309 expressed in most plant organs, *MtFPN2* transcripts were only detected in two discrete

310 nodule regions: associated to the nodule vasculature, and from late Zone II to early Zone

311 III. This dual localization indicates a dual function related with iron efflux from the cytosol,

312 as inferred from the yeast complementation assays and from the available information on

313 the biochemistry of this family of transporters.

314 In the vasculature, MtFPN2 would introduce iron into the lumen of an

315 endomembranous compartment. Considering the relatively large amount of iron that has to

316 be transferred across the nodule vessels into the nodules (González-Guerrero et al., 2014;

317 González-Guerrero et al., 2016), it could be argued that the endomembranes would serve as

318 an iron buffer, storing it prior to being delivered to the apoplast of the infection zone or to

319 be recycled back to the host in older parts of the nodule. It could also be hypothesized that

320 the iron concentrated in intracellular compartments could be released in the apoplast by

321 exocytosis, as it has been proposed for phosphate transport mediated by the PHO1 protein

322 (Arpat et al., 2012). It is unlikely that MtFPN2 would participate in a direct translocation of

323 iron from the cytosol across the plasma membrane, since no signal was observed using

324 immunolocalization and transmission electron microscopy. In contrast, the localization of

325 MtFPN2 in the symbiosome provides a clear insight into a key function for MtFPN2:

326 mediating iron delivery to the bacteroids.

327 Several evidences in addition to the expression and localization data support this

328 role. Loss of *MtFPN2* function leads to a reduction of nitrogen fixation capabilities, with

11

329 negative effects on plant growth, biomass production, and nodule development.

330 Nitrogenase activity is highly dependent on iron delivery, due to its large requirements of

331 iron for its three cofactors (Rubio and Ludden, 2005). Altering iron uptake by rhizobia-

332 infected nodule cells presented a similar phenotype, as shown when characterizing the

333 *nramp1-1 M. truncatula* mutant (Tejada-Jiménez et al., 2015). In addition, iron delivery to

334 *fpn2-1* nodules is affected in terms of total concentration, distribution in the nodule, and

335 speciation, indicating a large disturbance in nodule iron homeostasis. Altered nodule

336 development has also been reported when legumes were grown in iron-deficient substrates

337 (O'Hara et al., 1988; Tang et al., 1990; Tang et al., 1992), or when iron delivery was altered

338 by mutating iron transporters (Hakoyama et al., 2012; Tejada-Jiménez et al., 2015), or the

339 iron-chelation system (Stephens et al., 2011; Kryvoruchko et al., 2018). The changes in iron

340 speciation in *fpn2-1* nodules would be the consequence of several factors: i) iron being

341 stored or retained by iron-detoxification systems as a consequence of not reaching the

342 proper acceptors, ii) loss of signal from ferro-proteins that have not received their cofactor,

343 iii) mismetallation of proteins due to iron being retained in different compartments.

344 Although attempts were made to fit the spectra obtained with different iron-complex

345 reference standards, the complexity and number of these species made it extremely difficult

346 to conclude anything other than a reduction of iron-sulfur species in nodules, which would

347 very likely include the iron-sulfur clusters of nitrogenase. This phenotype was stronger in

348 white non-functional nodules, but also present in those with wild type colour, a leaky

349 phenotype that was also observed with *MtNramp1* mutants (Tejada-Jiménez et al., 2015)

350 and that might indicated the existence of secondary systems able to deliver, with low

351 affinity or non-specifically, some iron for nitrogen fixation in nodules.

352   The roles of MtFPN2 in the vasculature and in the symbiosomes were not equally

353 important. Expressing *MtFPN2* only in the nodule cortical cells was enough to at least

354 partially restore the wild-type phenotype. This means that facilitating iron transport across

355 the symbiosome membrane would be the key function of MtFPN2. In contrast, when

356 *MtFPN2* was only expressed in the vasculature, no significant improvements in plant

357 growth, nodule development, or nitrogenase activity were observed compared to the *fpn2-1*

358 nodules. This would also hint at the existence of mechanisms to deliver iron out of the

359 vessels that are independent of MtFPN2. In contrast, in the symbiosomes, MtFPN2 would

12

360   not be easily substituted by another iron transporter, including MtSEN1, which has also

361   been hypothesized to be in this membrane (Hakoyama et al., 2012). This would also

362   explain why the attempts to functionally complement *fpn2-1* by increasing iron content in

363   the nutrient solution did not work, since it would require to: i) accumulate at high enough

364   levels in the cell cytosol to overcome MtFPN2 absence without becoming toxic, and ii)

365   recruit another transporter that might use iron as a substrate although at lower affinities.

366   Overall, we now have a better understanding of the mechanisms of iron delivery for

367   symbiotic nitrogen fixation. Iron would be delivered by the vessels into the apoplast of the

368   infection/differentiation zone of the nodule (Rodríguez-Haas et al., 2013). Iron release from

369   the vessels would be facilitated by MtFPN2 and some other unknown protein(s). Once in

370   the apoplast, it would form a complex with the citrate released by MtMATE67

371   (Kryvoruchko et al., 2018). Then, a yet-to-be-determined ferroreductase must work to

372   convert Fe^{3+} into Fe^{2+} that is the substrate of MtNramp1, the protein responsible for iron

373   uptake by rhizobia-infected nodule cells (Tejada-Jiménez et al., 2015). Once in the cytosol,

374   iron will be sorted to different subcellular compartments. In the case of the symbiosome,

375   MtMATE67 would also be required to form the iron-citrate complexes that seem to be the

376   preferred iron species to be taken up by bacteroids (Moreau et al., 1995; Le Vier et al.,

377   1996).

378

379   **METHODS**

380   **Biological material and growth conditions**

381   *M. truncatula* R108 and *fpn2-1* seeds were scarified in concentrated sulfuric acid for

382   7.5 min (R108) or 6.5 min (*fpn2-1*). Excess acid was removed and washed away eight times

383   with cold water, followed by surface-sterilization in 50 % (v/v) bleach for 90 s. Sterilized

384   seeds were embedded in sterile water overnight in darkness. Seeds were stratified in water-

385   agar plates for 48 h at 4 ºC and germinated at 22 ºC. Seedlings were planted on sterile

386   perlite pots, and inoculated with *S. meliloti* 2011 or the same bacterial strain transformed

387   pHC60-GFP (Cheng and Walker, 1998). Plants were grown in a greenhouse under 16 h

388   light / 8 h dark at 25 ºC / 20 ºC conditions. In the case of perlite pots, plants were watered

389   every two days with Jenner's solution or water alternatively (Brito et al., 1994). Nodulated

390   plants were harvested at 28 dpi. For hairy-root transformation experiments, *M. truncatula*

391   seedling were transformed with *Agrobacterium rhizogenes* strain ARqua1, containing the

392   appropriate binary vector as described (Boisson-Dernier et al., 2001).

393   Yeast complementation assays were carried out using the *S. cerevisiae* strain *ccc1*

394   (MATa *ade2-1 his3-11 leu2-3,112, trp1-1, ura3-52 can1-100, ccc1::his3*) and parental

395   DY150 (MATa *ade2-1 his3-11 leu2-3,112, trp1-1, ura3-52 can1-100*). The strains were

396   grown in synthetic dextrose (SD) medium, supplemented with the required auxotrophic

397   nutrients, 2 % glucose as carbon source, and the iron concentration indicated in each

398   particular plate.

399   RNA Extraction and RT-qPCR

400   RNA was obtained from 28 dpi plants or equivalent age non-inoculated plants using

401   Tri-Reagent (Life Technologies), treated with DNase turbo (Life Technologies), and

402   cleaned with RNeasy Mini kit (Qiagen). Samples were tested for possible DNA

403   contamination by PCR using the RNA samples as templates and primers specific for *M.*

404   *truncatula Ubiquitin carboxyl-terminal hydrolase* (*Medtr4g077320.1*) (Supplemental Table

405   2). RNA integrity was confirmed by electrophoresis. cDNA was synthesized from 500 ng

406   of DNA-free RNA using PrimeScript RT reagent Kit (Takara), supplemented with RNase

407   out (Life Technologies).

408   Expression studies were carried out by real-time reverse transcription polymerase

409   chain reaction (RT-qPCR) using the StepOne plus thermocycler (Applied Biosystems),

410   using the Power SyBR Green master mix (Applied Biosystems). The primers used are

411   indicated in Supplemental Table 2. RNA levels were standardized using the *M. truncatula*

412   *Ubiquitin carboxyl-terminal hydrolase* (*Medtr4g077320.1*) gene. Real time cycler

413   conditions have been previously described (González-Guerrero et al., 2010). The threshold

414   cycle (Ct) was determined in triplicate from three different assays, each with at least pooled

415   material from three different plants). The relative levels of expression were determined

416   using the $2^{\Delta Ct}$ method. All assays contained a non-RT control to detect possible DNA

417   contaminations.

418   Yeast complementation assays

14

419   Restriction sites *PstI* and *XhoI* were added to *MtFPN2* cDNA by PCR using the

420   primers listed in Supplemental Table 2. The amplicon was inserted into the *PstI/XhoI* sites

421   of yeast expression vector pDR196 and cloned using T4 ligation. Yeast strains were

422   transformed with either the empty pDR196 or pDR196::*MtFPN2* using the lithium acetate

423   method (Schiestl and Gietz, 1989) and selected by uracil autotrophy. Complementation

424   assays were carried out in SD medium plates with the required auxotrophic nutrients. To

425   test tolerance to iron, the plates were supplemented with 2.5 mM $FeSO_4$.

426   **GUS Staining**

427   *MtFPN2* promoter region was obtained by amplifying the 2144 pb upstream of the

428   start codon using the primers Forward MtFPN2p-GW and Reverse MtFPN2p-GW

429   (Supplemental Table 2). The amplicon was cloned in pDONR2017 (Invitrogen) by

430   Gateway Technology (Invitrogen) and transferred to destination vector pGWB3 (Nakagawa

431   *et al.*, 2007). Hairy-root transformation of *M. truncatula* seedling was carried out as

432   indicated above. After three weeks on Fahreus medium supplemented with 50 µg/ml

433   kanamycin, the transformed plants were transferred to sterilized perlite pots and inoculated

434   with *S. meliloti* 2011. GUS activity was determined in root and nodules of 28 dpi plants as

435   described (Vernoud et al., 1999).

436   **Immunolocalization studies**

437   The coding sequence region of *MtFPN2* and the promoter region used in the GUS

438   staining were fused by PCR using the primers indicated in Supplemental Table 2. This

439   fragment was cloned in pDONR207 (Invitrogen) using Gateway Technology and

440   transferred to pGWB13 (three HA epitopes fused in C-terminus) (Nakagawa et al., 2007).

441   Hairy-root transformation was carried out as described previously (Boisson-Dernier et al.,

442   2001). Transformants were inoculated with *S. meliloti* 2011 containing the pHC60 plasmid

443   that constitutively expressed GFP. Nodules and roots were collected at 28 dpi.

444   Samples for immunolocalization with a confocal microscope were fixed in 4%

445   paraformaldehyde, 2.5 % sucrose in phosphate-buffered saline (PBS) solution at 4 ºC

446   overnight (12 – 16 h). Fixative was removed and samples washed twice. Nodule and roots

447   were included in 6 % agarose and then sectioned in a Vibratome 1000 Plus (Vibratome) in

448   100 - 150 µm thick slices. Sections were dehydrated by serial incubation with methanol (30

15

449   %, 50 %, 70 % and 100 % in PBS) for 5 min and then rehydrated following the same

450   methanol series in reverse order. Cell wall permeabilization was carried out by incubation

451   with 2 % cellulase in PBS for 1 h and 0.1 % Tween 20 for 15 min. Sections were blocked

452   with 5 % bovine serum albumin (BSA) in PBS and then incubated with 1:50 anti-HA

453   mouse monoclonal antibody (Sigma) in PBS at room temperature for 2 h. Primary antibody

454   was washed three times with PBS for 15 min and subsequently incubated with 1:40 Alexa

455   594 - conjugated anti-mouse rabbit monoclonal antibody (Sigma) in PBS at room

456   temperature for 1 h. Secondary antibody was washed three times with PBS for 10 min, and

457   then DNA was stained using DAPI. Images were obtained with a confocal laser-scanning

458   microscope (Leica SP8) using excitation light at 488 nm and 561 nm for GFP and Alexa

459   594, respectively. DAPI-stained zones were visualized with UV light.

460   Immunolocalization in an electron microscope was carried out with 28 dpi nodules

461   from MtFPN2-HA expressing plants fixed in 1 % formaldehyde, 0.5 % glutaraldehyde,

462   2.5% sucrose in 50 mM potassium phosphate buffer (pH 7.4) at 4 ºC for 14 – 16 h in gentle

463   agitation. Samples were dehydrated with ethanol series and embedded in LR-White resin

464   (London Resin Company Ltd, UK). Nodule were placed in gelatine capsules, filled with

465   LR-White resin and polymerized at 60 ºC for 24 h. Serial ultrathin sections were cut using a

466   diamond knife in a Reichert Ultracut S Ultramicrotrome (Leica). Sections for

467   immunolocalization were blocked with 2 % BSA on PBS for 30 min, then incubated with

468   1:50 anti-HA rabbit monoclonal antibody (Sigma) in PBS at room temperature for 3 h.

469   Primary antibody was washed ten times with PBS for 2 min and next incubated with 1:150

470   anti-rabbit goat monoclonal antibody conjugated to 15 nm gold particles (Fisher Scientific)

471   in PBS at room temperature for 1 h. Secondary antibody was washed ten times with PBS

472   for 2 min, after that samples were washed fifteen times with water for 2 min. Sections were

473   stained with 2 % uranyl acetate and visualized in a JEM 1400 electron microscope at 80 kV

474   at Centro Nacional de Microscopía Electrónica.

475   **Acetylene reduction assays**

476   The acetylene reduction assay was used to measure nitrogenase activity in 28 dpi

477   plants (Hardy et al., 1968). Wild type and *fpn2-1* roots with nodules were introduced in 30

478   ml vials fitted with rubber stoppers. Each tube contained four or five independently

16

479 transformed plants. Three milliliters of air of each bottle was replaced by the same volume

480 of acetylene. The vials were incubated for 30 min at room temperature, when 0.5 ml gas

481 samples were taken from each of the tube. Ethylene content in each sample was measured

482 in a Shimadzu GC-8A gas chromatograph using a Porapak N column. The amount of the

483 ethylene produced was determined by measuring the height of the ethylene peak relative to

484 standards.

Metal content determination

486 Iron content was determined in shoots, roots, and nodules 28 dpi. Plant tissues were

487 weighted and mineralized in 15.6 M HNO_3 (trace metal grade) for 1 h at 80 ºC and

488 overnight at 20 ºC. Digestions were completed with 2 M H_2O_2. Samples were diluted in

489 300 mM HNO_3 prior to measurements. Element analyses were performed with Atomic

490 Absorption Spectroscopy (AAS) in an AAnalyst 800 (Perkin Elmer), equipped with a

491 graphite furnace. All samples were measured in duplicate.

Synchrotron-based X-ray fluorescence and XANES

493 µXRF hyperspectral images and µXANES spectra were acquired on the beamline

494 ID21 of the European Synchrotron Radiation Facility (Cotte et al., 2017), at 110 K in the

495 liquid nitrogen (LN2) cooled cryostat of the Scanning X-ray Micro-spectroscopy end-

496 station. A nodule from each of at least five *M. truncatula* R108 or *fpn2-1* plants (totalling

497 five R108 nodules, five pink *fpn2-1* nodules, and five white *fpn2-1* nodules) were

498 embedded into OCT medium and cryo-fixed by plunging in isopentane chilled with LN2.

499 25 µm-thick sections of frozen samples were obtained using a Leica LN22 cryo-microtome

500 and accommodated in a Cu sample holder cooled with LN2, sandwiched between Ultralene

501 (SPEX SamplePrep) foils. The beam was focused to 0.4×0.9 µm^2 with a Kirkpatrick-Baez

502 (KB) mirror system. The emitted fluorescence signal was detected with energy-dispersive,

503 large area (80 mm^2) SDD detector equipped with Be window (XFlash SGX from RaySpec).

504 Images were acquired at the fixed energy of 7.2 keV, by raster-scanning the sample in the

505 X-ray focal plane, with a step of 2×2 µm^2 or 0.5×0.5 µm^2 and 100 ms dwell time.

506 Elemental mass fractions were calculated from fundamental parameters with the PyMca

507 software package, applying pixel-by-pixel spectral deconvolution to hyperspectral maps

508 normalized by the incoming current (Sole et al., 2007). The incoming flux was monitored

17

509   using a drilled photodiode previously calibrated by varying the photon flux at 7.2 KeV

510   obtaining a response of 1927.9 charges/photon with a linear response up to 200 kcps. In

511   PyMCA the incoming flux and XRF detector parameters were set to 2×10^9 photons/s,

512   0.7746 cm^2 active area, and 4.65 cm sample to XRF detector distance. Sample matrix was

513   assumed to be amorphous ice (11% H, 89% O, density 0.92 g/cm^3), the sample thickness

514   set at 25µm obtained with the use of a cryo-microtome.

515   Fe-K edge (7.050 to 7.165 keV energy range, 0.5 eV step) micro X-ray absorption

516   near edge spectroscopy (µXANES) spectra were recorded in regions of interest of the

517   fluorescence maps on ID21 beamline (ESRF, France). Individual spectra were processed

518   using Orange software with the Spectroscopy add-on (Demsar et al., 2013). The pre-

519   processing step consisted of vector normalization and a second derivative Savitsky-Golay

520   filter to highlight potential differences among genotypes. Then a principal component

521   analysis combined to a linear discriminant analysis (when there were more than two

522   conditions to compare) was performed on the second derivative of the spectra to highlight

523   potential differences among genotypes. Average spectra from the regions was then fitted

524   using a linear combination routine

525

Statistical tests

527   Data were analyzed by t-test to calculate statistical significance of observed

528   differences, between wild type plants and analyzed mutants. Test results with p-values

529   lower than 0.05 were considered as statistically significant.

530

ACKNOWLEDGEMENTS

539 of laboratory 281 at Centro de Biotecnología y Genómica de Plantas (UPM-INIA) for their

540 support and feedback in preparing this manuscript.

541

542 **AUTHOR CONTRIBUTION**

543 VE carried out most of the experimental work. IA, CL, JV, and HC-M generated the

544 synchrotron-based X-ray fluorescence, XANES, and X-ray tomographic data. JQ and JMA

545 were responsible for metal determinations. MT-J and ER-N executed the yeast

546 complementation assays. RP participated in *M. truncatula* transformation assays. JW and

547 KSM performed *M. truncatula* mutant screening and isolated the *fpn2-1* allele. VE, JI, and

548 MG-G were responsible for experimental design, data analyses, and wrote the manuscript.

549

550 **REFERENCES**

551 **Akkermans, M.D., van der Horst-Graat, J.M., Eussen, S.R.B.M., van Goudoever, J.B.,**
552 **and Brus, F.** (2016). Iron and Vitamin D deficiency in healthy young children in
553 Western-Europe despite current nutritional recommendations. J. Pediatr.
554 Gastroenterol. Nutr. **62**, 635-642

555 **Andaluz, S., Rodríguez-Celma, J., Abadía, A., Abadía, J., and López-Millán, A.F.**
556 (2009). Time course induction of several key enzymes in *Medicago truncatula* roots
557 in response to Fe deficiency. Plant Physiol. Biochem. **47,** 1082-1088.

558 **Appleby, C.A.** (1984). Leghemoglobin and *Rhizobium* respiration. Annu. Rev. Plant
559 Physiol. **35,** 443-478.

560 **Arpat, A.B., Magliano, P., Wege, S., Rouached, H., Stefanovic, A., and Poirier, Y.**
561 (2012). Functional expression of PHO1 to the Golgi and trans-Golgi network and its
562 role in export of inorganic phosphate. Plant J. **71,** 479-491.

563 **Boisson-Dernier, A., Chabaud, M., Garcia, F., Bécard, G., Rosenberg, C., and Barker,**
564 **D.G.** (2001). *Agrobacterium rhizogenes*-transformed roots of *Medicago truncatula*
565 for the study of nitrogen-fixing and endomycorrhizal symbiotic associations. Mol.
566 Plant Microbe Interact. **14,** 695-700.

567 **Brear, E.M., Day, D.A., and Smith, P.M.C.** (2013). Iron: an essential micronutrient for
568 the legume–rhizobium symbiosis. Front. Plant Sci. **4,** 359.

19

569   **Brito, B., Palacios, J.M., Hidalgo, E., Imperial, J., and Ruíz-Argüeso, T.** (1994). Nickel
570   availability to pea (*Pisum sativum* L.) plants limits hydrogenase activity of
571   *Rhizobium leguminosarum* bv. *viciae* bacteroids by affecting the processing of the
572   hydrogenase structural subunits. J. Bacteriol. **176,** 5297-5303.

573   **Catalano, C.M., Czymmek, K.J., Gann, J.G., and Sherrier, D.J.** (2006). *Medicago*
574   *truncatula* syntaxin SYP132 defines the symbiosome membrane and infection
575   droplet membrane in root nodules. Planta **225,** 541-550.

576   **Cheng, H.P., and Walker, G.C.** (1998). Succinoglycan is required for initiation and
577   elongation of infection threads during nodulation of alfalfa by *Rhizobium meliloti*. J.
578   Bacteriol. **180,** 5183-5191.

579   **Colangelo, E.P., and Guerinot, M.L.** (2004). The essential basic helix-loop-helix protein
580   FIT1 is required for the iron deficiency response. Plant Cell **16,** 3400-3412.

581   **Colangelo, E.P., and Guerinot, M.L.** (2006). Put the metal to the petal: metal uptake and
582   transport throughout plants. Curr. Opin. Plant Biol. **9,** 322-330.

583   **Conte, S., Stevenson, D., Furner, I., and Lloyd, A.** (2009). Multiple antibiotic resistance
584   in Arabidopsis is conferred by mutations in a chloroplast-localized transport protein.
585   Plant Physiol. **151,** 559.

586   **Cotte, M. P. E., Salomé, M. Rivard, C. Nolf, W. D., Castillo-Michel, H., Fabris, T.,**
587   **Monico, L., Janssens, K., Wang, T., Sciau, P., Verger, L., Cormier, L.,**
588   **Dargaud, O., Brun, E., Bugnazet, D., Fayard, B., Hesse, B., del Real, A. E. P.,**
589   **Veronesi, G., Langlois, J., Balcar, N., Vandenberghe, Y., Solé, V. A., Kieffer, J.,**
590   **Barrett, R., Cohen, C., Cornu, C., Baker, R., Gagliardini, E., Papillon, E.,**
591   **Susini, J.** (2017). The ID21 X-ray and infrared microscopy beamline at the ESRF:
592   status and recent applications to artistic materials. J. Anal. At. Spectrom. **32,** 477-
593   493.

594   **Curie, C., Panaviene, Z., Loulergue, C., Dellaporta, S.L., Briat, J.-F., and Walker,**
595   **E.L.** (2001). Maize yellow stripe1 encodes a membrane protein directly involved in
596   Fe(III) uptake. Nature **409,** 346-349.

597   **Dalton, D.A., Joyner, S.L., Becana, M., Iturbe-Ormaetxe, I., and Chatfield, J.M.**
598   (1998). Antioxidant defenses in the peripheral cell layers of legume root nodules.
599   Plant Physiol. **116,** 37-43.

600 **Demsar, J., Curk, T., Erjavec, A., Gorup, C., Hocevar, T., Milutinovic, M., Mozina,**
601   **M., Polajnar, M., Toplak, M., Staric, A., Stajdohar, M., Umek, L., Zagar, L.,**
602   **Zbontar, J., Zitnik, M., and Zupan, B.** (2013). Orange: Data mining toolbox in
603   Python. J. Machine Learning Res. **14,** 2349-2353.

604 **Downie, J.A.** (2014). Legume nodulation. Curr. Biol. **24,** R184-R190.

605 **Drakesmith, H., Nemeth, E., and Ganz, T.** (2015). Ironing out Ferroportin. Cell Metab.
606   **22,** 777-787.

607 **Durrett, T.P., Gassmann, W., and Rogers, E.E.** (2007). The FRD3-mediated efflux of
608   citrate into the root vasculature is necessary for efficient iron translocation. Plant
609   Physiol. **144,** 197-205.

610 **Flis, P., Ouerdane, L., Grillet, L., Curie, C., Mari, S., and Lobinski, R.** (2016).
611   Inventory of metal complexes circulating in plant fluids: a reliable method based on
612   HPLC coupled with dual elemental and high-resolution molecular mass
613   spectrometric detection. New Phytol. **211,** 1129-1141.

614 **Gage, D.J.** (2002). Analysis of infection thread development using Gfp- and DsRed-
615   expressing *Sinorhizobium meliloti*. J. Bacteriol. **184,** 7042-7046.

616 **Goldstein, S., Meyerstein, D., and Czapski, G.** (1993). The Fenton reagents. Free Radic.
617   Biol. Med. **15,** 435-445.

618 **González-Guerrero, M., Raimunda, D., Cheng, X., and Argüello, J.M.** (2010). Distinct
619   functional roles of homologous Cu$^+$ efflux ATPases in *Pseudomonas aeuginosa*.
620   Mol. Microbiol. **78,** 1246-1258.

621 **González-Guerrero, M., Matthiadis, A., Sáez, Á., and Long, T.A.** (2014). Fixating on
622   metals: new insights into the role of metals in nodulation and symbiotic nitrogen
623   fixation. Front. Plant Sci. **5,** 45.

624 **González-Guerrero, M., V., E., Sáez, Á., and Tejada-Jiménez, M.** (2016). Transition
625   metal transport in plants and associated endosymbionts. Arbuscular mycorrhizal
626   fungi and rhizobia. Front. Plant Sci. **7,** 1088.

627 **Grillet, L., Lan, P., Li, W., Mokkapati, G., and Schmidt, W.** (2018). IRON MAN is a
628   ubiquitous family of peptides that control iron transport in plants. Nature Plants **4,**
629   953-963.

21

630 **Hakoyama, T., Niimi, K., Yamamoto, T., Isobe, S., Sato, S., Nakamura, Y., Tabata, S.,**
631   **Kumagai, H., Umehara, Y., Brossuleit, K., Petersen, T.R., Sandal, N.,**
632   **Stougaard, J., Udvardi, M.K., Tamaoki, M., Kawaguchi, M., Kouchi, H., and**
633   **Suganuma, N.** (2012). The integral membrane protein SEN1 is required for
634   symbiotic nitrogen fixation in *Lotus japonicus* nodules. Plant Cell Physiol. **53,** 225-
635   236.

636 **Hardy, R.W., Holsten, R.D., Jackson, E.K., and Burns, R.C.** (1968). The acetylene-
637   ethylene assay for n(2) fixation: laboratory and field evaluation. Plant Physiol. **43,**
638   1185-1207.

639 **Herridge, D.F., Peoples, M.B., and Boddey, R.M.** (2008). Global inputs of biological
640   nitrogen fixation in agricultural systems. Plant Soil **311,** 1-18.

641 **Hirschi, K.D.** (2009). Nutrient Biofortification of Food Crops. Annu. Rev. Nutr. **29,** 401-
642   421.

643 **Huisman, R., Ovchinnikova, E., Bisseling, T., and Limpens, E.** (2012). Endocytic
644   Accommodation of Microbes in Plants (Berlin, Heidelberg: Springer Berlin
645   Heidelberg), pp. 271-295.

646 **Kaiser, B.N., Moreau, S., Castelli, J., Thomson, R., Lambert, A., Bogliolo, S., Puppo,**
647   **A., and Day, D.A.** (2003). The soybean NRAMP homologue, GmDMT1, is a
648   symbiotic divalent metal transporter capable of ferrous iron transport. Plant J. **35,**
649   295-304.

650 **Kaplan, J.** (2002). Mechanisms of cellular iron acquisition: Another iron in the fire. Cell
651   **111,** 603-606.

652 **Kereszt, A., Mergaert, P., and Kondorosi, E.** (2011). Bacteroid development in legume
653   nodules: Evolution of mutual benefit or of sacrificial victims? Mol. Plant-Microbe
654   Interact. **24,** 1300-1309.

655 **Kobayashi, T., and Nishizawa, N.K.** (2012). Iron uptake, translocation, and regulation in
656   higher plants. Annu. Rev. Plant Biol. **63,** 131-152.

657 **Korshunova, Y.O., Eide, D., Clark, W.G., Guerinot, M.L., and Pakrasi, H.B.** (1999).
658   The IRT1 protein from *Arabidopsis thaliana* is a metal transporter with a broad
659   substrate range. Plant Mol. Biol. **40,** 37-44.

660 **Kryvoruchko, I.S., Routray, P., Sinharoy, S., Torres-Jerez, I., Tejada-Jiménez, M.,**
661 **Finney, L.A., Nakashima, J., Pislariu, C.I., Benedito, V.A., González-Guerrero,**
662 **M., Roberts, D.M., and Udvardi, M.K.** (2018). An iron-activated citrate
663 transporter, MtMATE67, is required for symbiotic nitrogen fixation. Plant Physiol.
664 **176,** 2315-2329.

665 **Kumar, R.K., Chu, H.-H., Abundis, C., Vasques, K., Rodriguez, D.C., Chia, J.-C.,**
666 **Huang, R., Vatamaniuk, O.K., and Walker, E.L.** (2017). Iron-nicotianamine
667 transporters are required for proper long distance iron signaling. Plant Physiol. **175,**
668 1254.

669 **Le Vier, K., Day D.A., and Guerinot M.L.** (1996). Iron uptake by symbiosomes from
670 soybean root nodules. Plant Physiol. **111, 893-900**

671 **Li, L., Chen, O.S., Ward, D.M., and Kaplan, J.** (2001). CCC1 is a transporter that
672 mediates vacuolar iron storage in yeast. J. Biol. Chem. **276,** 29515-29519.

673 **Limpens, E., Ivanov, S., van Esse, W., Voets, G., Fedorova, E., and Bisseling, T.**
674 (2009). *Medicago* N$_2$-fixing symbiosomes acquire the endocytic identity marker
675 Rab7 but delay the acquisition of vacuolar identity. Plant Cell **21,** 2811-2828.

676 **Lin, H., Li, L., Jia, X., Ward, D.M., and Kaplan, J.** (2011). Genetic and biochemical
677 analysis of high iron toxicity in yeast: Iron toxicity is due to the accumulation of
678 cytosolic iron and occurs under both aerobic and anaerobic conditions. J. Biol.
679 Chem. **286,** 3851-3862.

680 **Long, T.A., Tsukagoshi, H., Busch, W., Lahner, B., Salt, D.E., and Benfey, P.N.**
681 (2010). The bHLH transcription factor POPEYE regulates response to iron
682 deficiency in Arabidopsis roots. Plant Cell **22,** 2219-2236.

683 **López-Millán, A.-F., Morales, F.n., Abadía, A., and Abadía, J.** (2000). Effects of iron
684 deficiency on the composition of the leaf apoplastic fluid and xylem sap in sugar
685 beet. Implications for iron and carbon transport. Plant Physiol. **124,** 873-884.

686 **Magne, K., Couzigou, J.-M., Schiessl, K., Liu, S., George, J., Zhukov, V., Sahl, L.,**
687 **Boyer, F., Iantcheva, A., Mysore, K.S., Wen, J., Citerne, S., Oldroyd, G.E.D.,**
688 **and Ratet, P.** (2018). *MtNODULE ROOT1* and *MtNODULE ROOT2* are essential
689 for indeterminate nodule identity. Plant Physiol. **178,** 295.

690 **Marschner, P.** (2011). Mineral Nutrition of Higher Plants 3rd Edition. (Academic Press).

691 **McKie, A.T., Marciani, P., Rolfs, A., Brennan, K., Wehr, K., Barrow, D., Miret, S.,**
692 **Bomford, A., Peters, T.J., Farzaneh, F., Hediger, M.A., Hentze, M.W., and**
693 **Simpson, R.J.** (2000). A novel duodenal Iron-Regulated transporter, IREG1,
694 implicated in the basolateral transfer of iron to the circulation. Mol. Cell **5,** 299-309.

695 **Montiel, J., Arthikala, M.-K., Cárdenas, L., and Quinto, C.** (2016). Legume NADPH
696 oxidases have crucial roles at different stages of nodulation. Int. J. Mol. Sci. **17,**
697 680.

698 **Montiel, J., Nava, N., Cárdenas, L., Sánchez-López, R., Arthikala, M.-K., Santana, O.,**
699 **Sánchez, F., and Quinto, C.** (2012). A *Phaseolus vulgaris* NADPH oxidase gene is
700 required for root infection by rhizobia. Plant Cell Physiol. **53,** 1751-1767.

701 **Moreau, S., Meyer J.M., and Puppo A.** (1995). Uptake of iron by symbiosomes and
702 bacteroids from soybean nodules. FEBS Lett. **361,** 225-228.

703 **Morrissey, J., Baxter, I.R., Lee, J., Li, L., Lahner, B., Grotz, N., Kaplan, J., Salt, D.E.,**
704 **and Guerinot, M.L.** (2009). The ferroportin metal efflux proteins function in iron
705 and cobalt homeostasis in Arabidopsis. Plant Cell **21,** 3326-3338.

706 **Mus, F., Crook, M.B., Garcia, K., Garcia Costas, A., Geddes, B.A., Kouri, E.D.,**
707 **Paramasivan, P., Ryu, M.H., Oldroyd, G.E., Poole, P.S., Udvardi, M.K., Voigt,**
708 **C.A., Ane, J.M., and Peters, J.W.** (2016). Symbiotic nitrogen fixation and
709 challenges to extending it to non-legumes. Appl. Environ. Microbiol. **82,** 3698-
710 3710.

711 **Nakagawa, T., Kurose, T., Hino, T., Tanaka, K., Kawamukai, M., Niwa, Y., Toyooka,**
712 **K., Matsuoka, K., Jinbo, T., and Kimura, T.** (2007). Development of series of
713 gateway binary vectors, pGWBs, for realizing efficient construction of fusion genes
714 for plant transformation. J. Biosci. Bioeng. **104,** 34-41.

715 **Nevo, Y., and Nelson, N.** (2006). The NRAMP family of metal-ion transporters. Biochim.
716 Biophys. Acta **1763,** 609-620.

717 **O'Hara, G.W., Dilworth, M.J., Boonkerd, N., and Parkpian, P.** (1988). Iron-deficiency
718 specifically limits nodule development in peanut inoculated with Bradyrhizobium
719 sp. New Phytologist **108,** 51-57.

720 **Oldroyd, G.E., and Dixon, R.** (2014). Biotechnological solutions to the nitrogen problem.
721 Curr. Opin. Biotechnol. **26,** 19-24.

24

722 **Preisig, O., Zufferey, R., and Hennecke, H.** (1996a). The *Bradyrhizobium japonicum*
723   fixGHIS genes are required for the formation of the high-affinity cbb(3)-type
724   cytochrome oxidase. Arch. Microbiol. **165,** 297-305.

725 **Preisig, O., Zufferey, R., Thony-Meyer, L., Appleby, C., and Hennecke, H.** (1996b). A
726   high-affinity cbb3-type cytochrome oxidase terminates the symbiosis- specific
727   respiratory chain of *Bradyrhizobium japonicum.* J. Bacteriol. **178,** 1532-1538.

728 **Rodríguez-Haas, B., Finney, L., Vogt, S., González-Melendi, P., Imperial, J., and**
729   **González-Guerrero, M.** (2013). Iron distribution through the developmental stages
730   of *Medicago truncatula* nodules. Metallomics **5,** 1247-1253.

731 **Rogers, E.E., and Guerinot, M.L.** (2002). FRD3, a member of the multidrug and toxin
732   efflux family, controls iron deficiency responses in Arabidopsis. Plant Cell **14,**
733   1787-1799.

734 **Roschzttardtz, H., Séguéla-Arnaud, M., Briat, J.-F., Vert, G., and Curie, C.** (2011).
735   The FRD3 citrate effluxer promotes iron nutrition between symplastically
736   disconnected tissues throughout Arabidopsis development. Plant Cell **23,** 2725-
737   2737.

738 **Roux, B., Rodde, N., Jardinaud, M.-F., Timmers, T., Sauviac, L., Cottret, L., Carrère,**
739   **S., Sallet, E., Courcelle, E., Moreau, S., Debellé, F., Capela, D., de Carvalho-**
740   **Niebel, F., Gouzy, J., Bruand, C., and Gamas, P.** (2014). An integrated analysis
741   of plant and bacterial gene expression in symbiotic root nodules using laser-capture
742   microdissection coupled to RNA sequencing. Plant J. **77,** 817-837.

743 **Rubio, L.M., and Ludden, P.W.** (2005). Maturation of nitrogenase: a biochemical puzzle.
744   J. Bacteriol. **187,** 405-414.

745 **Rubio, M.C., James, E.K., Clemente, M.R., Bucciarelli, B., Fedorova, M., Vance, C.P.,**
746   **and Becana, M.** (2004). Localization of superoxide dismutases and hydrogen
747   peroxide in legume root nodules. Mol. Plant Microbe Int. **17,** 1294-1305.

748 **Schiestl, R.H., and Gietz, R.D.** (1989). High efficiency transformation of intact yeast cells
749   using single stranded nucleic acids as carrier. Curr. Genet. **16,** 339-346.

750 **Sivitz, A.B., Hermand, V., Curie, C., and Vert, G.** (2012). Arabidopsis bHLH100 and
751   bHLH101 control iron homeostasis via a FIT-independent pathway. PLoS ONE **7,**
752   e44843.

753 **Solé, V. A., Papillon, E., Cotte, M., Walter, P., Susini, J. A**. (2007). A multiplatform
754   code for the analysis of energy-dispersive X-ray fluorescence spectra
755   Spectrochimica Acta Part B: Atomic Spectroscopy **62,** 63-68.

756 **Sprent, J.I.** (2007). Evolving ideas of legume evolution and diversity: a taxonomic
757   perspective on the occurrence of nodulation. New Phytol. **174,** 11-25.

758 **Stephens, B., Cook, D., and Grusak, M.** (2011). Characterization of zinc transport by
759   divalent metal transporters of the ZIP family from the model legume *Medicago*
760   *truncatula*. Biometals **24,** 51-58.

761 **Sutton, W.D., Pankhurst, C.E., and Craig, A.S.** (1981). The Rhizobium Bacteroid State.
762   In Biology of the Rhizobiaceae, K.L. Atherly and G. Gilesalan, eds (Academic
763   Press CY -), pp. 149-177.

764 **Tadege, M., Wen, J., He, J., Tu, H., Kwak, Y., Eschstruth, A., Cayrel, A., Endre, G.,**
765   **Zhao, P.X., Chabaud, M., Ratet, P., and Mysore, K.S.** (2008). Large-scale
766   insertional mutagenesis using the Tnt1 retrotransposon in the model legume
767   *Medicago truncatula*. Plant J. **54,** 335-347.

768 **Tang, C., Robson, A.D., and Dilworth, M.J.** (1990). The role of iron in nodulation and
769   nitrogen fixation in *Lupinus angustifolius* L. New Phytol. **114,** 173-182.

770 **Tang, C.X., Robson, A.D., Dilworth, M.J., and Kuo, J.** (1992). Microscopic evidence on
771   how iron-deficiency limits nodule initiation in *Lupinus angustifolius* l. New Phytol.
772   **121,** 457-467.

773 **Tejada-Jiménez, M., Castro-Rodríguez, R., Kryvoruchko, I., Lucas, M.M., Udvardi,**
774   **M., Imperial, J., and González-Guerrero, M.** (2015). *Medicago truncatula*
775   Natural Resistance-Associated Macrophage Protein1 is required for iron uptake by
776   rhizobia-infected nodule cells. Plant Physiol. **168,** 258-272.

777 **Tejada-Jiménez, M., Gil-Diez, P., Leon-Mediavilla, J., Wen, J., Mysore, K.S.,**
778   **Imperial, J., and Gonzalez-Guerrero, M.** (2017). *Medicago truncatula*
779   molybdate transporter type 1 (MOT1.3) is a plasma membrane molybdenum
780   transporter required for nitrogenase activity in root nodules under molybdenum
781   deficiency. New Phytol **216,** 1223-1235.

782   **Terry, R.E., Soerensen, K.U., Jolley, V.D., and Brown, J.C.** (1991). The role of active
783   *Bradyrhizobium japonicum* in iron stress response of soy-beans. Plant Soil **130,**
784   225-230.

785   **Udvardi, M., and Poole, P.S.** (2013). Transport and metabolism in legume-rhizobia
786   symbioses. Annu. Rev. Plant Biol. **64,** 781-805.

787   **Vance, C.P.** (2001). Symbiotic nitrogen fixation and phosphorus acquisition. Plant
788   nutrition in a world of declining renewable resources. Plant Physiol. **127,** 390-397.

789   **Vasse, J., de Billy, F., Camut, S., and Truchet, G.** (1990). Correlation between
790   ultrastructural differentiation of bacteroids and nitrogen fixation in alfalfa nodules.
791   J. Bacteriol. **172,** 4295-4306.

792   **Vernié, T., Kim, J., Frances, L., Ding, Y., Sun, J., Guan, D., Niebel, A., Gifford, M.L.,**
793   **de Carvalho-Niebel, F., and Oldroyd, G.E.D.** (2015). The NIN transcription
794   factor coordinates diverse nodulation programs in different tissues of the *Medicago*
795   *truncatula* root. Plant Cell**, 27**, 3410-3420.

796   **Vernoud, V., Journet, E.P., and Barker, D.G.** (1999). *MtENOD20*, a Nod factor-
797   inducible molecular marker for root cortical cell activation. Mol. Plant Microbe
798   Interact. **12,** 604-614.

799   **Vert, G., Grotz, N., Dedaldéchamp, F., Gaymard, F., Guerinot, M.L., Briat, J.F., and**
800   **Curie, C.** (2002). IRT1, an *Arabidopsis* transporter essential for iron uptake from
801   the soil and the plant growth. Plant Cell **14,** 1223-1233.

802   **von Wiren, N., Klair, S., Bansal, S., Briat, J.-F., Khodr, H., Shioiri, T., Leigh, R.A.,**
803   **and Hider, R.C.** (1999). Nicotianamine chelates both FeIII and FeII. Implications
804   for metal transport in plants. Plant Physiol. **119,** 1107-1114.

805   **White, P.J., and Broadley, M.R.** (2009). Biofortification of crops with seven mineral
806   elements often lacking in human diets - iron, zinc, copper, calcium, magnesium,
807   selenium and iodine. New Phytol. **182,** 49-84.

808   **Xiao, T.T., Schilderink, S., Moling, S., Deinum, E.E., Kondorosi, E., Franssen, H.,**
809   **Kulikova, O., Niebel, A., and Bisseling, T.** (2014). Fate map of *Medicago*
810   *truncatula* root nodules. Development **141,** 3517-3528.

811   **Zhai, Z., Gayomba, S.R., Jung, H.-i., Vimalakumari, N.K., Piñeros, M., Craft, E.,**
812   **Rutzke, M.A., Danku, J., Lahner, B., Punshon, T., Guerinot, M.L., Salt, D.E.,**

813   **Kochian, L.V., and Vatamaniuk, O.K.** (2014). OPT3 Is a phloem-specific iron

814   transporter that is essential for systemic iron signaling and redistribution of iron and

815   cadmium in *Arabidopsis*. Plant Cell **26,** 2249-2264.

816

817

818

819

820

821

822   **FIGURE LEGENDS**

823   **Figure 1.** *MtFPN2* is expressed in the vasculature and in the differentiation-fixation zones

824   of *M. truncatula* nodules. (A) *MtFPN2* expression in nodulated or nitrogen-fertilized *M.*

825   *truncatula* plants relative to the internal standard gene *Ubiquitin carboxyl-terminal*

826   *hydrolase*. Data are the mean ± SE of two independent experiments with 4 pooled plants.

827   (B) GUS staining of 28 dpi *M. truncatula* nodules expressing the *gus* gene under the

828   control of *MtFPN2* promoter region. Bar = 500 μm. (C) Longitudinal section of a GUS-

829   stained 28 dpi *M. truncatula* nodule expressing the *gus* gene under the *MtFPN2* promoter

830   region. ZI indicates Zone I; ZII, Zone II; IZ, Interzone; and ZIII, Zone III. Bar = 100 μm.

831   (D) Cross section of a GUS-stained 28 dpi *M. truncatula* nodule expressing the *gus* gene

832   under the *MtFPN2* promoter region. Bar = 100 μm.

833   **Figure 2.** MtFPN2 is localized in intracellular membranes in the vasculature and in the

834   symbiosome membrane in *S. meliloti*-infected nodule cells. (A) Longitudinal section of a

835   28 dpi *M. truncatula* nodule expressing *MtFPN2-HA* under its own promoter. The three C-

836   terminal HA epitopes were detected using an Alexa594-conjugated antibody (red, left

837   panel). Transformed plants were inoculated with a GFP-expressing *S. meliloti* strain (green,

838   middle panel). Both images were overlaid with the channel showing DAPI-stained DNA

839   (blue, right panel). Bar = 100 μm. (B) Cross section of a vessel of 28 dpi *M. truncatula*

840   nodule expressing *MtFPN2-HA* under its own promoter. The three C-terminal HA epitopes

28

841   were detected using an Alexa594-conjugated antibody (red, left panel). Transillumination

842   image is shown in the centre panel, and overlaid with the Alexa594 signal (right panel). Bar

843   = 25 µm. (C) Detail of a *S. meliloti*-colonized 28 dpi nodule cell in the differentiation zone.

844   Right panel shows the Alexa594 signal (red), middle panel the *S. meliloti* distribution

845   (green), and the right one overlays both images. Bar = 10 µm. (D). Detail of symbiosomes

846   shown by transmission electron microscopy (left panel). Arrows indicate the position of the

847   colloidal gold particles conjugated to the antibody used to detect MtFPN2-HA. Middle

848   panel, *M. truncatula* nodule vessel shown with transmission electron microscopy. Asterisks

849   indicate the position of the xylem. Boxed region was amplified in the right panel to show

850   the antibody-conjugated gold particles used to position MtFPN2-HA (indicated by arrows).

851   **Figure 3.** MtFPN2 transports iron out of the cytosol. Parental yeast strain DY150 was

852   transformed with the pDR196 empty vector, while the *ccc1* mutant was transformed with

853   either pDR196 or pDR196 harbouring the *MtFPN2* coding sequence. Serial dilutions (10x)

854   of the transformants were grown in YPD medium (top panel), SD medium with the

855   required auxotrophies (centre panel), or in SD medium with the required auxotrophies and

856   2.5 mM FeSO$_4$ (lower panel).

857   **Figure 4.** MtFPN2 is required for symbiotic nitrogen fixation. (A) *Tnt1* insertion in the

858   fourth exon of *MtFPN2* results in no expression being detected by RT-PCR. The *Ubiquitin*

859   *carboxyl-terminal hydrolase* (MtUb1) gene was used as a positive control. (B) Growth of

860   representative wild type (WT), *fpn2-1*, and *fpn2-1* transformed with the *MtFPN2* coding

861   sequence expressed under its own promoter (*FPN2$_{prom}$::MtFPN2*). Bar = 1 cm. (C) Detail

862   of representative nodules of WT, *fpn2-1*, and *FPN2$_{prom}$::MtFPN2*-transformed *fpn2-1*

863   plants. Bars = 500 µm. (D) Number of pink or white nodules in 28 dpi WT, *fpn2-1*, and

864   *FPN2$_{prom}$::MtFPN2*-transformed *fpn2-1* plants. Data are the mean ± SE of at least 7

865   independently transformed plants. (E) Fresh weight of WT, *fpn2-1*, and

866   *FPN2$_{prom}$::MtFPN2*-transformed *fpn2-1* plants. Data are the mean ± SE of at least 7

867   independently transformed plants. (F) Nitrogenase activity in 28 dpi nodules from WT,

868   *fpn2-1*, and *FPN2$_{prom}$::MtFPN2*-transformed *fpn2-1* plants. Acetylene reduction was

869   measured in duplicate from two sets of four pooled plants. Data are the mean ± SE. (G)

870   Iron content in roots, shoot, and nodules of 28 dpi WT, *fpn2-1*, and *FPN2$_{prom}$::MtFPN2*-

29

871   transformed *fpn2-1* plants. Data are the mean ± SE of 3 sets of 4 pooled plants. * indicates

872   statistically significant differences (p < 0.05).

873   **Figure 5.** *MtFPN2* loss-of-function alters iron distribution and speciation in 28 dpi nodules.

874   (A). Synchrotron-based X-ray fluorescence images of wild type (left), pink *fpn2-1* (middle),

875   and white *fpn2-1* (right) nodules, showing calcium (top panels) or iron (lower panels)

876   distribution. Bars = 200 µm, intensity scale in mass fraction units (g/g). (B) XANES

877   spectra obtained from different regions of wild-type, pink *fpn2-1*, and white *fpn2-1* nodules

878   (top left panel). This signal was decomposed into its two principal components for Zone II

879   (top right panel), Zone III (lower left panel), and the vasculature (lower right panel). Green

880   represents wild-type samples; red, pink *fpn2-1*; and blue, white *fpn2-1* nodules.

881   **Figure 6.**   *MtFPN2* expression in cortical nodule cells partially restores the *fpn2-1*

882   phenotype. (A) Growth of representative wild type (WT), *fpn2-1*, and *fpn2-1* transformed

883   with the *MtFPN2* coding sequence expressed under the *MtMOT1.3* promoter

884   (*MOT1.3_{prom}::MtFPN2*). Bar = 1 cm. (B) Detail of representative nodules of WT, *fpn2-1*,

885   and *MOT1.3_{prom}::MtFPN2*-transformed *fpn2-1* plants. Bars = 500 µm. (C) Number of pink

886   or white nodules in 28 dpi WT, *fpn2-1*, and *MOT1.3_{prom}::MtFPN2*-transformed *fpn2-1*

887   plants. Data are the mean ± SE of at least 11 independently transformed plants. (D) Fresh

888   weight of WT, *fpn2-1*, and *MOT1.3_{prom}::MtFPN2*-transformed *fpn2-1* plants. Data are the

889   mean ± SE of at least 11 independently transformed plants. (E) Nitrogenase activity in 28

890   dpi nodules from WT, *fpn2-1*, and *MOT1.3_{prom}::MtFPN2*-transformed *fpn2-1* plants.

891   Acetylene reduction was measured in duplicate from two sets of four pooled plants. Data

892   are the mean ± SE. * indicates statistically significant differences (p < 0.05).
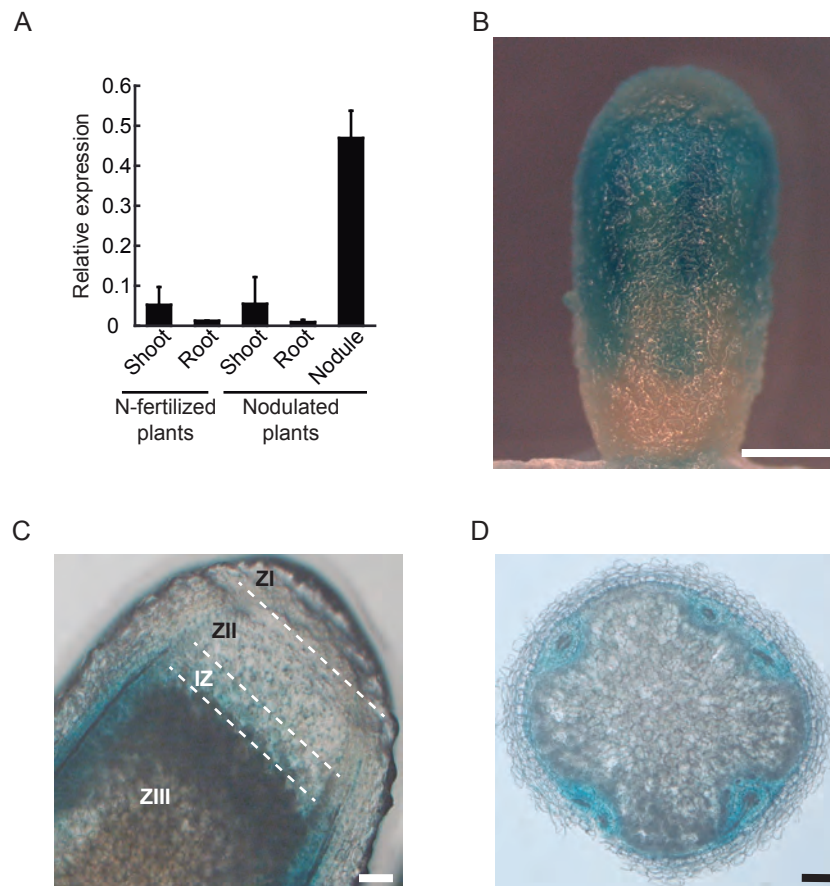
30

FIGURE 1

Figure 1. *MtFPN2* is expressed in the vasculature and in the differentiation-fixation zones of *M. truncatula* nodules. (A) *MtFPN2* expression in nodulated or nitrogen-fertilized *M. truncatula* plants relative to the internal standard gene *Ubiquitin carboxyl-terminal hydrolase*. Data are the mean ± SE of two independent experiments with 4 pooled plants. (B) GUS staining of 28 dpi *M. truncatula* nodules expressing the *gus* gene under the control of *MtFPN2* promoter region. Bar = 500 μm. (C) Longitudinal section of a GUS-stained 28 dpi *M. truncatula* nodule expressing the *gus* gene under the *MtFPN2* promoter region. ZI indicates Zone I; ZII, Zone II; IZ, Interzone; and ZIII, Zone III. Bar = 100 μm. (D) Cross section of a GUS-stained 28 dpi *M. truncatula* nodule expressing the *gus* gene under the MtFPN2 promoter region. Bar = 100 μm.
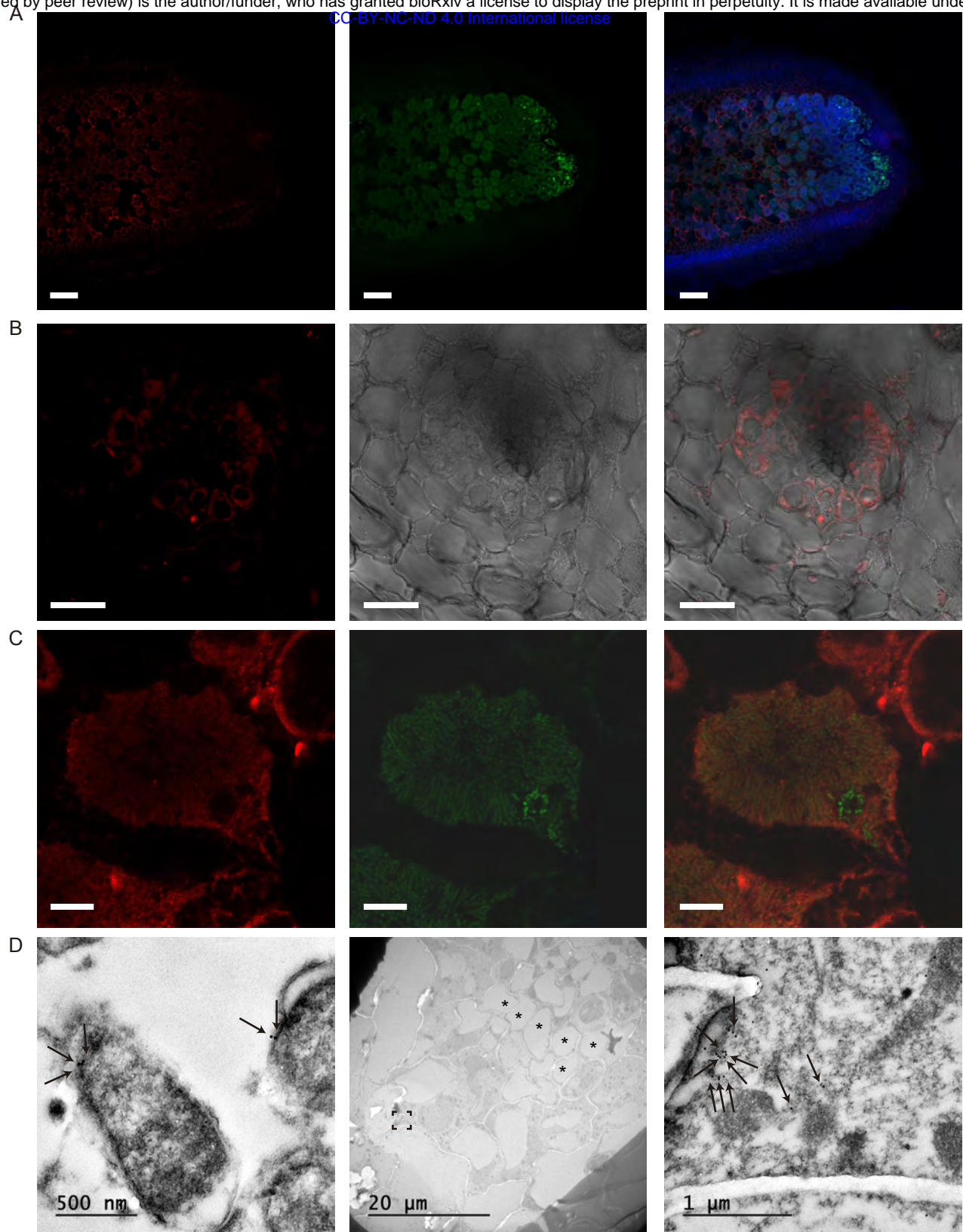
FIGURE 2

Figure 2. MtFPN2 is localized in intracellular membranes in the vasculature and in the symbiosome membrane in *S. meliloti*-infected nodule cells. (A) Longitudinal section of a 28 dpi *M. truncatula* nodule expressing *MtFPN2-HA* under its own promoter. The three C-terminal HA epitopes were detected using an Alexa594-conjugated antibody (red, left panel). Transformed plants were inoculated with a GFP-expressing *S. meliloti* strain (green, middle panel). Both images were overlaid with the channel showing DAPI-stained DNA (blue, right panel). Bar=100 μm. (B) Cross section of a vessel of 28 dpi *M. truncatula* nodule expressing *MtFPN2-HA* under its own promoter. The three C-terminal HA epitopes were detected using an Alexa594-conjugated antibody (red, left panel). Transillumination image is shown in the centre panel, and overlaid with the Alexa594 signal (right panel). Bar = 25 μm. (C) Detail of a *S. meliloti*-colonized 28 dpi nodule cell in the differentiation zone. Right panel shows the Alexa594 signal (red), middle panel the *S. meliloti* distribution (green), and the right one overlays both images. Bar = 10 μm. (D). Detail of symbiosomes shown by transmission electron microscopy (left panel). Arrows indicate the position of the colloidal gold particles conjugated to the antibody used to detect MtFPN2-HA. Middle panel, *M. truncatula* nodule vessel shown with transmission electron microscopy. Asterisks indicate the position of the xylem. Boxed region was amplified in the right panel to show the antibody-conjugated gold particles used to position MtFPN2-HA (indicated by arrows).
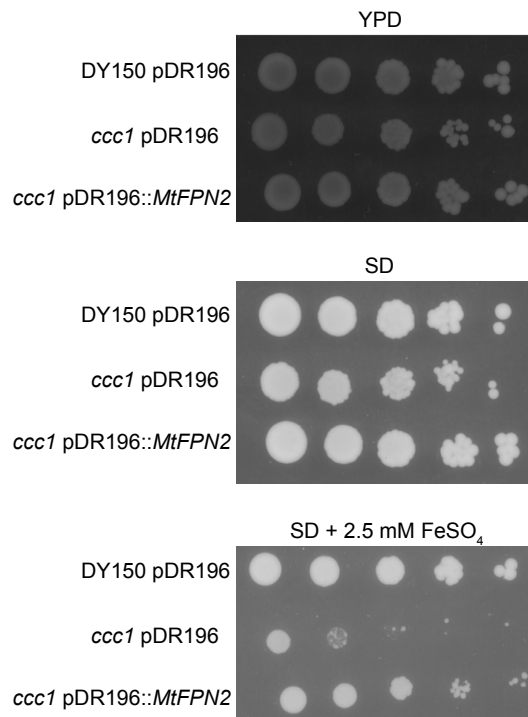
FIGURE 3

Figure 3. MtFPN2 transports iron out of the cytosol. Parental yeast strain DY150 was transformed with the pDR196 empty vector, while the *ccc1* mutant was transformed with either pDR196 or pDR196 harbouring the *MtFPN2* coding sequence. Serial dilutions (10x) of the transformants were grown in YPD medium (top panel), SD medium with the required auxotrophies (centre panel), or in SD medium with the required auxotrophies and 2.5 mM $FeSO_4$ (lower panel).
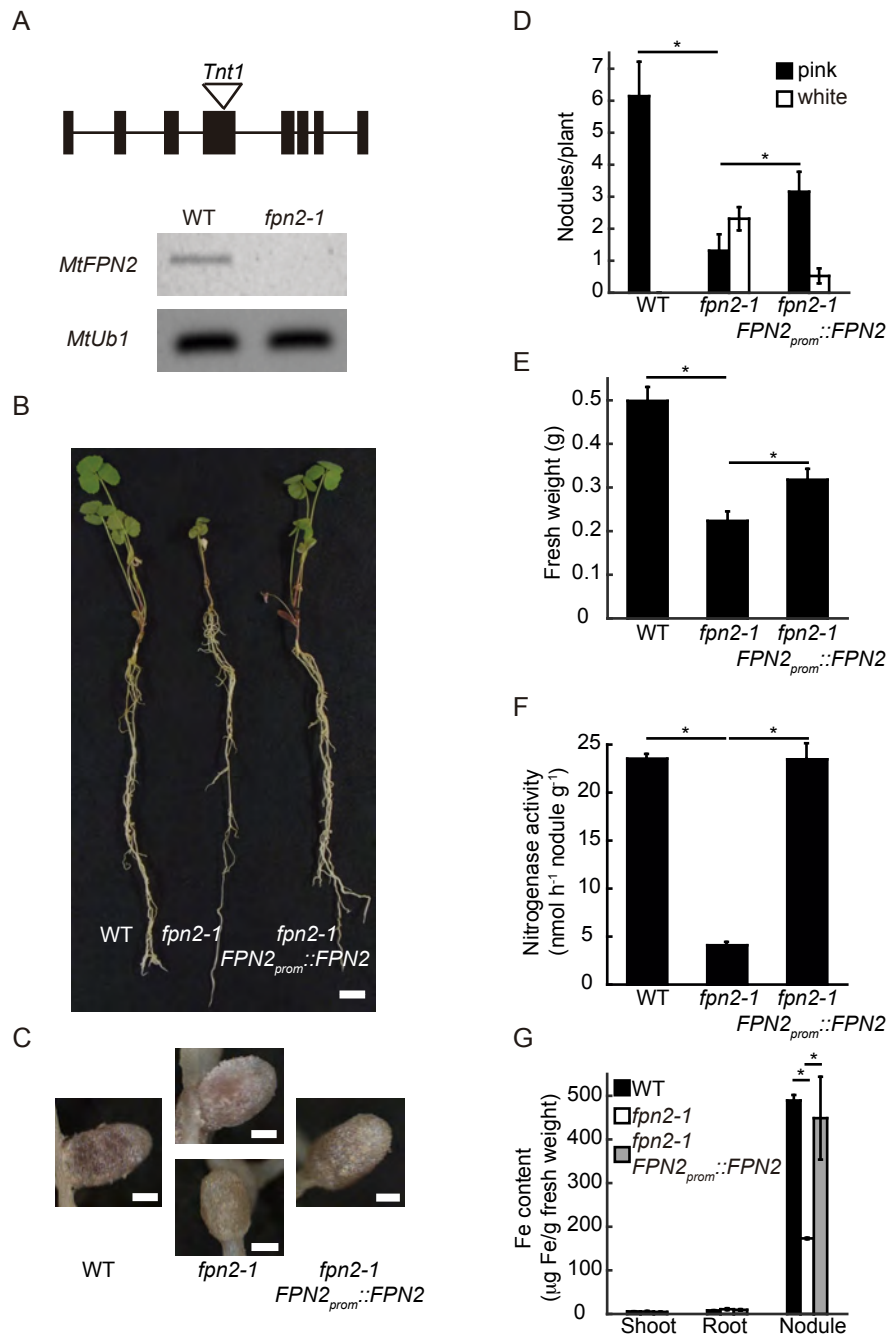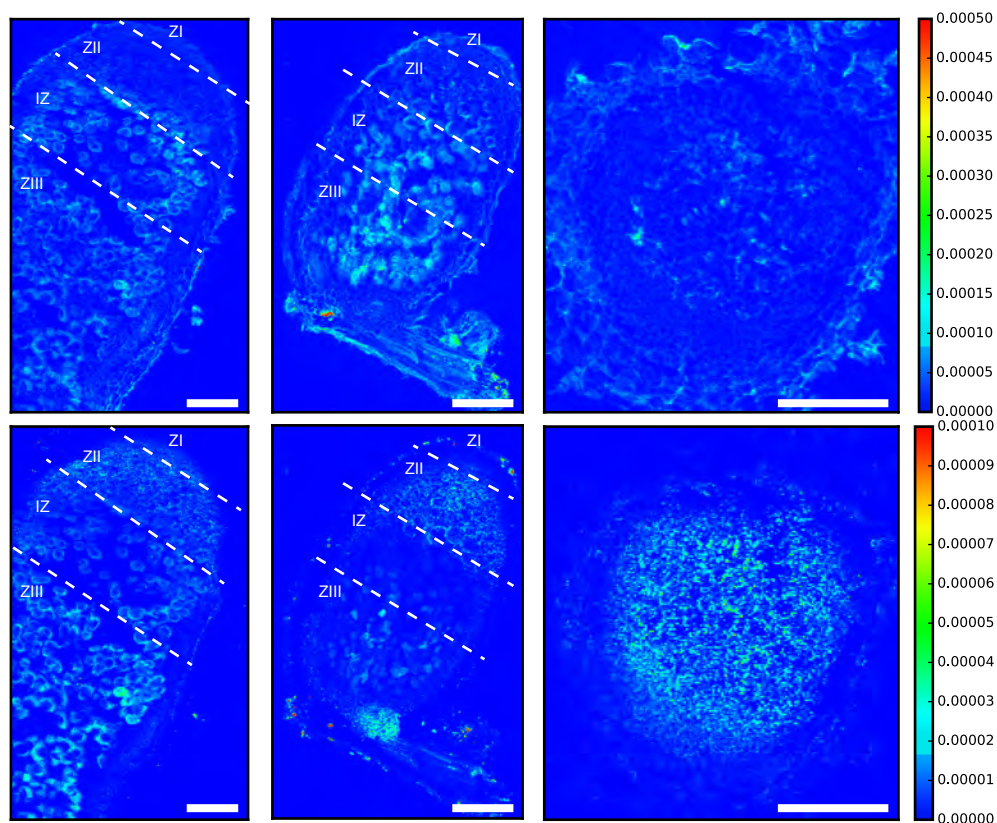
FIGURE 4

Figure 4. MtFPN2 is required for symbiotic nitrogen fixation. (A) *Tnt1* insertion in the fourth exon of *MtFPN2* results in no expression being detected by RT-PCR. The *Ubiquitin carboxyl-terminal hydrolase* (*MtUb1*) gene was used as a positive control. (B) Growth of representative wild type (WT), *fpn2-1*, and *fpn2-1* transformed with the *MtFPN2* coding sequence expressed under its own promoter ($FPN2_{prom}::MtFPN2$). Bar = 1 cm. (C) Detail of representative nodules of WT, *fpn2-1*, and $FPN2_{prom}::MtFPN2$-transformed *fpn2-1* plants. Bars = 500 μm. (D) Number of pink or white nodules in 28 dpi WT, *fpn2-1*, and $FPN2_{prom}::MtFPN2$-transformed *fpn2-1* plants. Data are the mean ± SE of at least 7 independently transformed plants. (E) Fresh weight of WT, *fpn2-1*, and $FPN2_{prom}::MtFPN2$-transformed fpn2-1 plants. Data are the mean ± SE of at least 7 independently transformed plants. (F) Nitrogenase activity in 28 dpi nodules from WT, *fpn2-1*, and $FPN2_{prom}::MtFPN2$-transformed fpn2-1 plants. Acetylene reduction was measured in duplicate from two sets of four pooled plants. Data are the mean ± SE. (G) Iron content in roots, shoot, and nodules of 28 dpi WT, *fpn2-1*, and $FPN2_{prom}::MtFPN2$-transformed *fpn2-1* plants. Data are the mean ± SE of 3 sets of 4 pooled plants. * indicates statistically significant differences (p < 0.05).
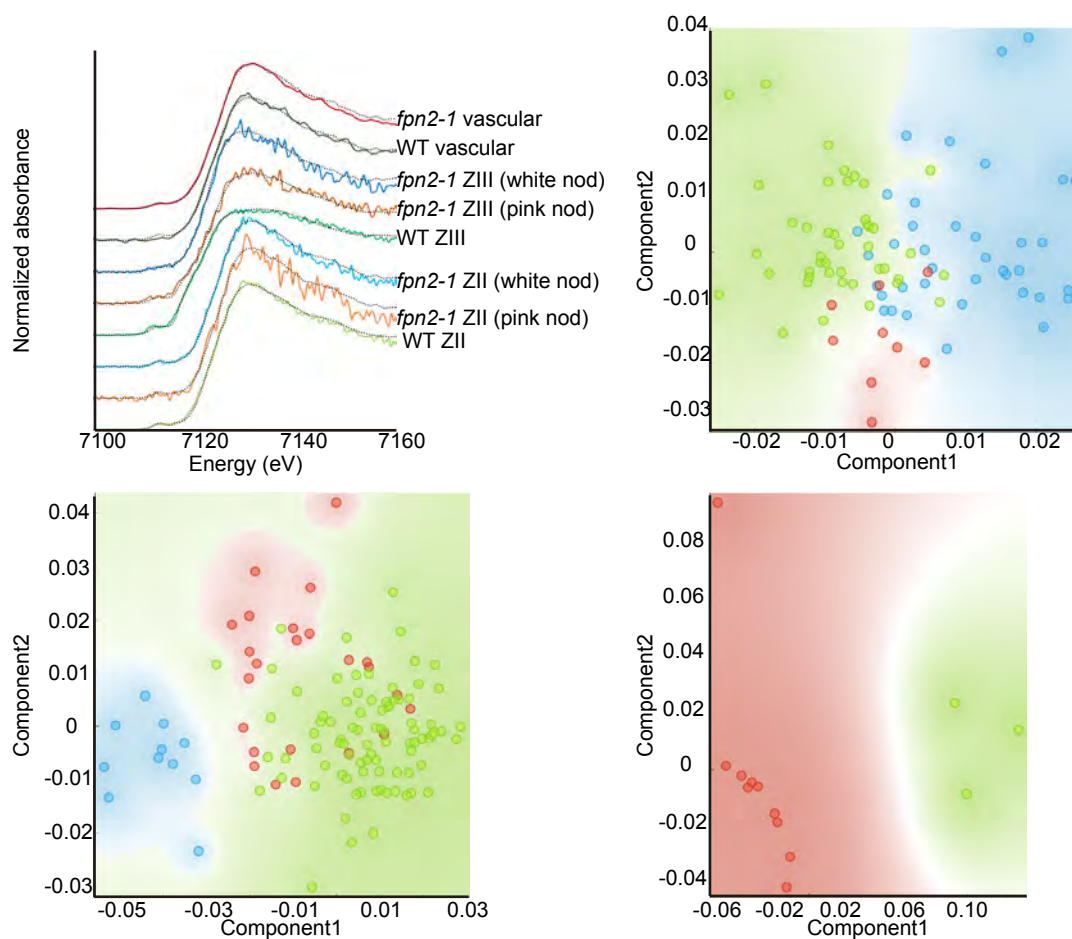
FIGURE 5

Figure 5. *MtFPN2* loss-of-function alters iron distribution and speciation in 28 dpi nodules. (A). Synchrotron-based X-ray fluorescence images of wild type (left), pink *fpn2-1* (middle), and white *fpn2-1* (right) nodules, showing calcium (top panels) or iron (lower panels) distribution. Bars = 200 µm, intensity scale in mass fraction units (g/g). (B) XANES spectra obtained from different regions of wild-type, pink *fpn2-1*, and white *fpn2-1* nodules (top left panel). This signal was decomposed into its two principal components for Zone II (top right panel), Zone III (lower left panel), and the vasculature (lower right panel). Green represents wild-type samples; red, pink *fpn2-1*; and blue, white *fpn2-1* nodules.
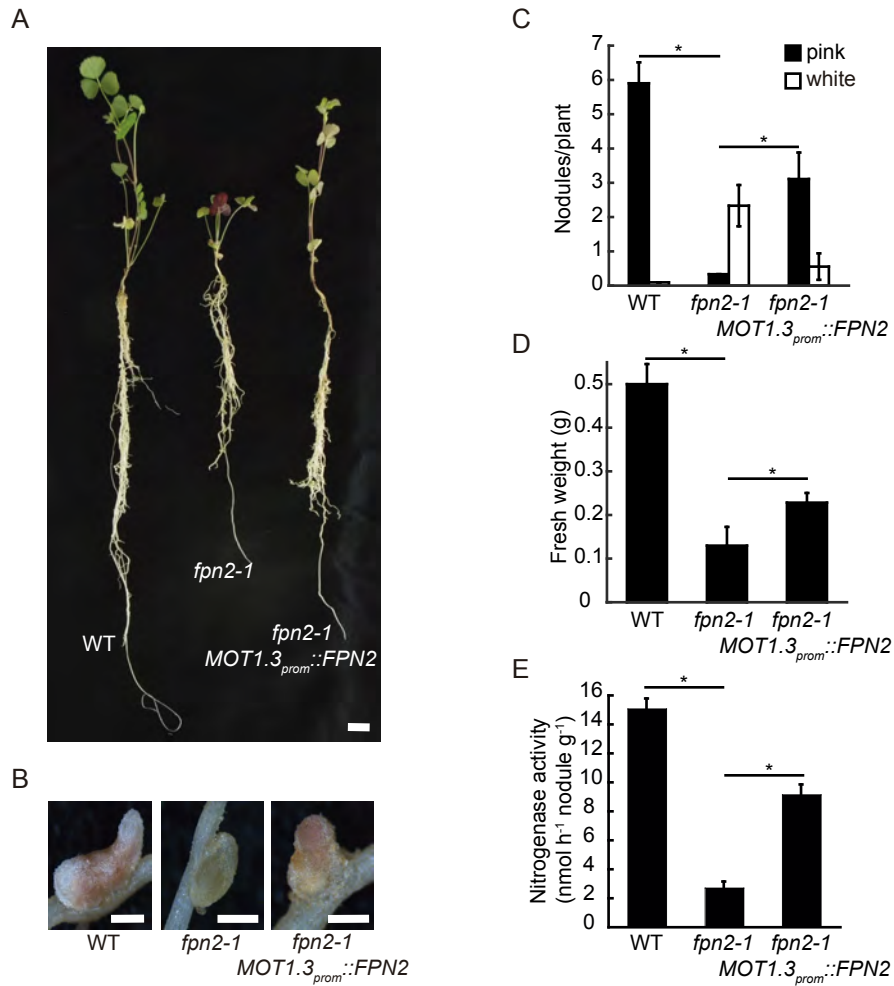
FIGURE 6

Figure 6. *MtFPN2* expression in cortical nodule cells partially restores the *fpn2-1* phenotype. (A) Growth of representative wild type (WT), *fpn2-1*, and *fpn2-1* transformed with the *MtFPN2* coding sequence expressed under the *MtMOT1.3* promoter (*MOT1.3prom::MtFPN2*). Bar = 1 cm. (B) Detail of representative nodules of WT, *fpn2-1*, and *MOT1.3prom::MtFPN2*-transformed *fpn2-1* plants. Bars = 500 µm. (C) Number of pink or white nodules in 28 dpi WT, *fpn2-1*, and *MOT1.3prom::MtFPN2*-transformed *fpn2-1* plants. Data are the mean ± SE of at least 11 independently transformed plants. (D) Fresh weight of WT, *fpn2-1*, and *MOT1.3prom::MtFPN2*-transformed *fpn2-1* plants. Data are the mean ± SE of at least 11 independently transformed plants. (E) Nitrogenase activity in 28 dpi nodules from WT, *fpn2-1*, and *MOT1.3prom::MtFPN2*-transformed *fpn2-1* plants. Acetylene reduction was measured in duplicate from two sets of four pooled plants. Data are the mean ± SE. * indicates statistically significant differences ($p < 0.05$).